High-bandwidth and flexible tracking control for precision motion with application to a piezo nanopositioner

Zhao Feng, , Jie Ling, , Min Ming, and , and Xiao-Hui Xiao

Citation: Review of Scientific Instruments **88**, 085107 (2017); doi: 10.1063/1.4998303
View online: http://dx.doi.org/10.1063/1.4998303
View Table of Contents: http://aip.scitation.org/toc/rsi/88/8
Published by the American Institute of Physics

High-bandwidth and flexible tracking control for precision motion with application to a piezo nanopositioner

Zhao Feng, Jie Ling, Min Ming, and Xiao-Hui Xiao[a)]
Hubei Key Laboratory of Waterjet Theory and New Technology, Wuhan University, Wuhan 430072, China

(Received 13 April 2017; accepted 30 July 2017; published online 15 August 2017)

For precision motion, high-bandwidth and flexible tracking are the two important issues for significant performance improvement. Iterative learning control (ILC) is an effective feedforward control method only for systems that operate strictly repetitively. Although projection ILC can track varying references, the performance is still limited by the fixed-bandwidth Q-filter, especially for triangular waves tracking commonly used in a piezo nanopositioner. In this paper, a wavelet transform-based linear time-varying (LTV) Q-filter design for projection ILC is proposed to compensate high-frequency errors and improve the ability to tracking varying references simultaneously. The LVT Q-filter is designed based on the modulus maximum of wavelet detail coefficients calculated by wavelet transform to determine the high-frequency locations of each iteration with the advantages of avoiding cross-terms and segmenting manually. The proposed approach was verified on a piezo nanopositioner. Experimental results indicate that the proposed approach can locate the high-frequency regions accurately and achieve the best performance under varying references compared with traditional frequency-domain and projection ILC with a fixed-bandwidth Q-filter, which validates that through implementing the LTV filter on projection ILC, high-bandwidth and flexible tracking can be achieved simultaneously by the proposed approach. *Published by AIP Publishing.* [http://dx.doi.org/10.1063/1.4998303]

I. INTRODUCTION

Many modern industrial equipment and scientific instruments, such as atomic force microscopes (AFMs),[1] scanning tunneling microscopes (SPMs),[2] information storage,[3] and wafer stages,[4] require precision motion, especially for accuracy at microscale and below. Primarily, high bandwidth and tracking flexibility are the two key issues in these systems. Taking the nanopositioner in AFMs as an example, the triangular waves with high acceleration of one axis to generate raster scanning result in high frequency errors, which requires a higher bandwidth of the system.[5] Furthermore, due to the variance of tracking reference caused by uncertainty of the sample surface, the system should be insensitive to reference variation. To tackle these issues, the implementation of the controller plays an important role on precision motion systems.[6]

Feedback controllers, such as resonant control (RC),[7] positive position feedback (PPF) control,[8] integral resonant control (IRC),[9] and H_∞ control,[10] have been implemented to improve bandwidth. However, because of some practical and fundamental algebraic restrictions in feedback, the bandwidth with feedback alone is still confined within the first resonant frequency.[11] To achieve high bandwidth and significant performance enhancement, the implementation of a feedforward controller is a key component.[12,13]

Iterative learning control (ILC) has found widespread applications, and the repetitive tracking errors as well as disturbances can be compensated by learning from the previous iterations and updating the control signal for the next iteration.[14,15] ILC can be designed by either the norm-optimal method or the frequency-domain approach.[14] For the norm-optimal method, the control force is determined by weighting matrices, and the tuning process may be cumbersome. Besides, with the increase of the sample rate and trajectory length, the large lifted matrices make it computationally costly or infeasible.[16] In contrast, the low-complexity frequency-domain ILC is suitable for practical implementation. To achieve a balance between tracking performance and robustness, a low-pass Q-filter is generally adopted. A high cut-off frequency of the Q-filter can improve the tracking bandwidth at the cost of deteriorating the performance for magnifying the noise and errors caused by model uncertainties, and vice-versa. To handle the problem, linear time-varying (LTV) Q-filters with time-varying bandwidth profile were proposed via analyzing tracking errors by time-frequency decomposition[17–19] and the locations for high cut-off frequency were fixed and pre-designed under repetitive reference input. However, on one hand, the change of reference during iterations will deteriorate tracking the performance significantly for flexible tracking. On the other hand, the fixed LTV bandwidth profile cannot meet high bandwidth tracking for all references because the location of high frequency errors may vary with input trajectories. In this regard, the traditional frequency-domain ILC with or without a LTV Q-filter has low ability for flexible tracking.

In order to enhance the ability to tracking varying references, in Refs. 20 and 21, different tasks were constructed by the repeated basic tasks trained by ILC and the optimal control signal was obtained by fitting the relevant basic tasks to realize flexible tracking. It should be noted that the tracking references are limited by the numbers of the basic tasks. As an alternative, norm-optimal ILC with basis function has been proposed by parameterizing the control signal via constructing finite impulse response (FIR) filters[22,23] or infinite impulse response (IIR) filters[24,25] during iterations. However, these

a)Author to whom correspondence should be addressed: xhxiao@whu.edu.cn.

methods still suffer from large computation of matrices and extra tedious iterations to obtain the parameters.[25]

Recently, a low-complexity frequency-domain projection ILC[26] has been proposed to avoid large computation and time-consuming tuning by projecting the error signal into the subspace by basis functions to maintain tracking flexibility.[27,28] Although the development of projection ILC has improved the ability of flexible tracking, the tracking bandwidth is still limited by the fixed linear time-invariant (LTI) Q-filter. Moreover, the time-frequency decomposition approaches to design a LTV Q-filter in Refs. 18 and 19 may be unpractical for the low extrapolation ability in traditional ILC framework.

The paper is motivated by high-bandwidth and flexible tracking for precision motion in many applications and relaxing the restrictions in traditional ILC. In this paper, a wavelet transform-based LTV Q-filter design for projection ILC is proposed to achieve high-bandwidth and flexible tracking simultaneously to overcome the above deficiencies. Instead of removing non-repetitive errors and disturbances,[29,30] the discrete wavelet transform (DWT) is utilized to determine the locations of high frequency regions by calculating the modulus maximum of the wavelet coefficients. Then, the LTV Q-filter is designed after each iteration with the advantage of avoiding the cross-terms and segmenting signals manually in Wigner-Ville time-frequency distribution. The projection ILC with a LTV Q-filter is also developed with experimental verification on a piezo nanopositioner in this paper.

The rest paper is organized as follows. In Sec. II, the system description and relative background is presented. The design of the proposed approach is described in Sec. III. Experiments on a piezo nanopositioner and comparisons of the results are elaborated in Sec. IV and Sec. V concludes the paper.

II. PROBLEM FORMULATION

A. System description

In this paper, a single-input-single-output (SISO), discrete-time and LTI system $P(z)$ with forward time-shift operator z is considered in Fig. 1. A two-degree freedom configuration is adopted, where the feedback controller $C_{fb}(z)$ is designed to retain stability and attenuate unknown disturbances and nonlinearity, and the feedforward control signal uff_i is developed to compensate repetitive reference-induced errors and disturbances. The control force u_i is determined by the sum of the feedforward control signal uff_i and feedback control signal ufb_i. y_i is the measured output when the anticipated trajectory input is r_i during iteration i with unknown noise v_i.

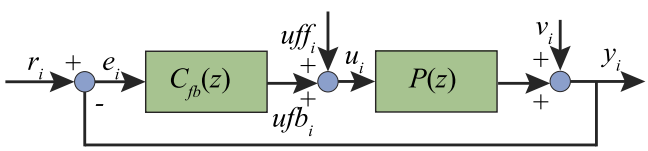

FIG. 1. Block diagram of the feedback-feedforward control scheme.

Considering the signal sequences with length N, the output at time $k \in \{0, 1, \ldots, N-1\}$ can be expressed as

$$y_i(k) = P(z)u_i(k) + v_i(k). \tag{1}$$

Alternatively, Eq. (1) can also be presented in lifted domain and the dynamics of $P(z)$ is equivalent to a $N \times N$ dimensional lifted matrix with

$$\underbrace{\begin{bmatrix} y_i(0) \\ y_i(1) \\ \vdots \\ y_i(N-1) \end{bmatrix}}_{\boldsymbol{y}_i} = \underbrace{\begin{bmatrix} h(0) & 0 & \ldots & 0 \\ h(1) & h(0) & \ldots & 0 \\ \vdots & \vdots & \vdots & \vdots \\ h(N-1) & h(N-2) & \ldots & h(0) \end{bmatrix}}_{\boldsymbol{P}} \times \underbrace{\begin{bmatrix} u_i(0) \\ u_i(1) \\ \vdots \\ u_i(N-1) \end{bmatrix}}_{\boldsymbol{u}_i} + \underbrace{\begin{bmatrix} v_i(0) \\ v_i(1) \\ \vdots \\ v_i(N-1) \end{bmatrix}}_{\boldsymbol{v}_i}, \tag{2}$$

where the coefficients $h(0)$, $h(1)$, …, $h(N-1)$ denote the impulse response sequences of $P(z)$, given by

$$P(z) \approx h(0) + h(1)z^{-1} + h(2)z^{-2} + \cdots + h(N-1)z^{-(N-1)}. \tag{3}$$

B. Projection ILC

The control law of traditional frequency-domain ILC generating the feedforward control signal is given by

$$uff_{i+1}(k) = Q(z)(uff_i(k) + L(z)e_i(k)), \tag{4}$$

where $Q(z)$ is a low-pass filter to improve robustness and $L(z)$ is the learning filter.[14] The convergence condition of the control signal is expressed as

$$\|Q(z)(1 - L(z)S(z)P(z))\|_\infty < 1, \tag{5}$$

where $S(z) = (1 + C_{fb}(z)P(z))^{-1}$ is the sensitive transfer function. The proof is proposed in Ref. 31 for details. According to Fig. 1, the error at iteration i and $i+1$ under $v_i = 0$ can be expressed, respectively, as

$$e_i(k) = S(z)r_i(k) - S(z)P(z)uff_i(k), \tag{6}$$

$$e_{i+1}(k) = S(z)r_{i+1}(k) - S(z)P(z)uff_{i+1}(k). \tag{7}$$

Suppose that $L(z) = (S(z)P(z))^{-1}$, $Q(z) = 1$, and $r_i(k) \neq r_{i+1}(k)$. By substituting Eqs. (4) and (6) to Eq. (7) and rearranging terms, it can be deduced that

$$e_{i+1}(k) = S(z)(r_{i+1}(k) - r_i(k)), \tag{8}$$

which reveals that traditional frequency-domain ILC is sensitive to reference variation and the performance is deteriorated significantly under flexible tracking.

To achieve flexible tracking, a projection step is adopted to approximate uff_{i+1} based on the control law of traditional frequency-domain ILC.[26] Define the cost criterion as

$$\boldsymbol{J}(\boldsymbol{\theta}_{i+1}) = \left\| \hat{e}_{i+1} - \hat{e}_{i+1}^{proj}(\theta_{i+1}) \right\|^2, \tag{9}$$

where $\hat{e}_{i+1}$ and $\hat{e}_{i+1}^{proj}$ are the estimated errors of the next iteration denoted as

$$\hat{e}_{i+1}(k) = e_i(k) - S(z)P(z)(uff_{i+1}(k) - uff_i(k)), \tag{10}$$

$$\hat{\boldsymbol{e}}_{i+1}^{proj}(k, \boldsymbol{\theta}_{i+1}) = e_i(k) - S(z)P(z)(C_{ff}(z, \boldsymbol{\theta}_{i+1})r_i(k) - uff_i(k)), \tag{11}$$

with the parameterized n-order FIR filter structure

$$C_{ff}(z, \boldsymbol{\theta}_{i+1}) = \sum_{j=1}^{n} \boldsymbol{\theta}_{i+1}[j]z^{-j}, \tag{12}$$

here, $\boldsymbol{\theta}_{i+1}$ is the parametric vector of the FIR filter coefficients. In lifted domain, Eq. (12) can also be rewritten as

$$\boldsymbol{C}_{ff}(\boldsymbol{\theta}_{i+1}) = \sum_{j=1}^{n} \boldsymbol{\psi}_j \boldsymbol{\theta}_{i+1}[j], \tag{13}$$

where $\boldsymbol{\psi}_j$ is the lifted matrix of z^{-j}. Hence, Eq. (9) can be expressed in time-domain as

$$\boldsymbol{J}(\boldsymbol{\theta}_{i+1}) = \left\| \boldsymbol{SPuff}_{i+1} - \boldsymbol{SP}\boldsymbol{\psi}_{\boldsymbol{r}_i}\boldsymbol{\theta}_{i+1} \right\|^2, \tag{14}$$

with $\boldsymbol{\psi}_{\boldsymbol{r}_i} = [\boldsymbol{\psi}_1\boldsymbol{r}_i, \boldsymbol{\psi}_2\boldsymbol{r}_i, \ldots, \boldsymbol{\psi}_n\boldsymbol{r}_i]$. By minimizing Eq. (14) using linear least squares, the optimal coefficients are obtained as

$$\boldsymbol{\theta}_{i+1}^{*} = (\boldsymbol{\psi}_{\boldsymbol{SPr}_i}^{\boldsymbol{T}}\boldsymbol{\psi}_{\boldsymbol{SPr}_i})^{-1}\boldsymbol{\psi}_{\boldsymbol{SPr}_i}^{\boldsymbol{T}}\boldsymbol{SPuff}_{i+1}, \tag{15}$$

where $\boldsymbol{\psi}_{\boldsymbol{SPr}_i} = [\boldsymbol{SP}\boldsymbol{\psi}_1\boldsymbol{r}_i, \boldsymbol{SP}\boldsymbol{\psi}_2\boldsymbol{r}_i, ..., \boldsymbol{SP}\boldsymbol{\psi}_n\boldsymbol{r}_i]$. Therefore, the feedforward control force by projection for next iteration is calculated by

$$u_{i+1}(k) = C_{ff}(z, \boldsymbol{\theta}_{i+1}^{*})r_{i+1}(k). \tag{16}$$

The block scheme of projection ILC is depicted in Fig. 2. For the design of $L(z)$, an approximate inversion method can be adopted to approximate $P(z)/(S(z)P(z))$ for fast convergence. The fixed-bandwidth $Q(z)$ is determined through trial-and-error to meet the performance. The selection of parameterized $C_{ff}(z)$ is depended on the references. In this paper, to improve the flexibility sufficiently, a FIR filter is constructed to project the signals for triangular waves tracking. Through designing $L(z)$ and $Q(z)$ primarily, the initial condition of projection ILC is given by setting the parametric vector of the FIR filter coefficients to zero and the plant is controlled by the feedback controller alone for the first iteration.

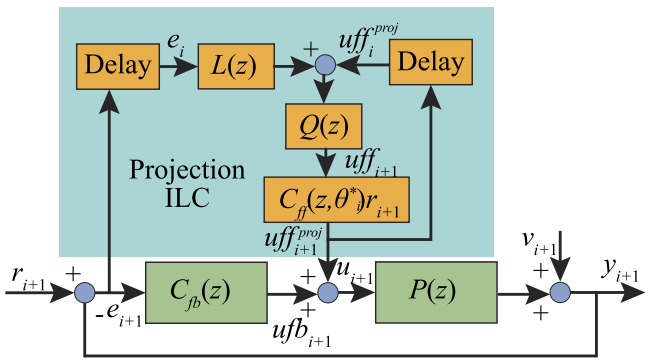

FIG. 2. Block scheme of projection ILC.

It should be noted that although projection ILC can track varying references, the tracking bandwidth is still limited by the fixed cut-off frequency of $Q(z)$.[18] The contradiction between high-bandwidth tracking and magnification of noise and unknown disturbances exists intrinsically. The design of $Q(z)$ with LTV bandwidth profile for projection ILC has not been explored deeply. The main difficulty lies in the determination of the locations of high frequency of errors for varying references, which the methods in Refs. 18 and 19 cannot handle.

C. Contribution of this paper

In brief, at present, the traditional frequency-domain ILC requires a system to execute repetitive reference, and the design of projection ILC has not taken high-bandwidth tracking into consideration. In view of the requirements in precision motion, the contributions of this paper are listed as below.

(1) The wavelet transform-based LTV Q-filter design method for flexible tracking is proposed to determine the locations of high-frequency regions of errors.
(2) The framework of combining the LTV Q-filter with projection ILC is developed for high-bandwidth and flexible tracking simultaneously.
(3) The proposed method is verified on a piezo nanopositioner under varying triangular waves.

III. WAVELET TRANSFORM-BASED TIME-VARYING FILTER DESIGN

A. Discrete wavelet transform

To analyze the error signal of each iteration, a time-frequency distribution is suitable for the advantages of capturing both frequency and location information over Fourier transform.[32] In this paper, the discrete wavelet transform (DWT) is adopted to locate the high frequency regions for its less computation and practical implementation compared with the continuous wavelet transform (CWT). Moreover, being different from the Wigner-Ville[18] or piece-wise Wigner[17] time-frequency distribution, DWT avoids the cross-term and manual segmentation of signals, which improves the accuracy and practicability of the proposed method.

DWT utilizes the analysis filter banks to decompose a signal into wavelet coefficients under various sub-band frequency ranges. The diagram of a 3-level wavelet decomposition is showed in Fig. 3(a). H and G represent high-pass and low-pass analysis wavelet filters, respectively. $\downarrow 2$ denotes the down sampling by a factor of two. cA is named as the approximation coefficients, which contains the low-frequency information that can retrieve the approximation of the signal. cD_1, cD_2, and cD_3 are the detail coefficients which contain the details of the signal in higher sub-band frequency ranges.

The choice of the filter bank level hinges on the desired frequency band resolution. In general, for a p-level wavelet decomposition, the sub-band frequency range of approximation coefficients is calculated by

$$f_{cA} = [0, 2^{-(p+1)}fs], \tag{17}$$

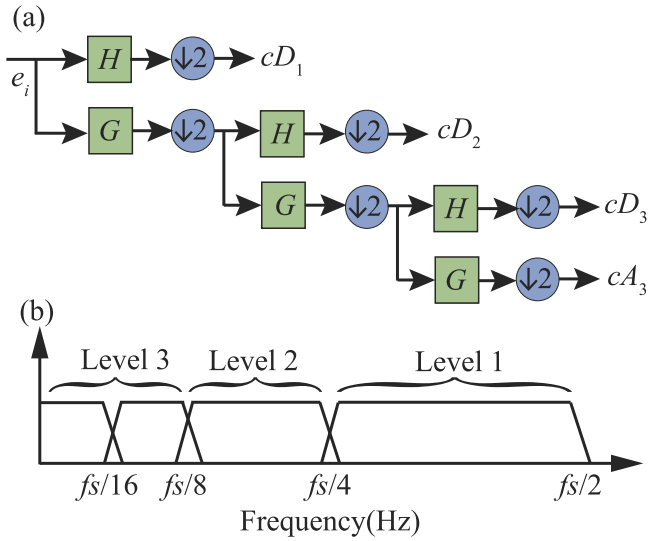

FIG. 3. Diagram of 3-level wavelet decomposition. (a) 3-level analysis filter banks. (b) Sub-band frequency ranges of DWT.

where fs is the sample rate in Hertz. The sub-band frequency ranges of detail coefficients can be expressed as

$$f_{cD_q} = [2^{-(q+1)}fs,\ 2^{-q}fs], \tag{18}$$

with $q \in \{1, \ldots, p\}$. A sub-band frequency range of 3-level wavelet decomposition is demonstrated in Fig. 3(b).

It should be noted that only the analysis filter banks for wavelet decomposition are used in this paper and the choice of wavelet function is based on the conformity of the original signal and the reconstructed signal of DWT.[29] For the purpose of locating high-frequency errors, the detail coefficients containing high-frequency information are utilized, which is different from the method to remove non-repetitive errors by adjusting wavelet coefficients through multiple experiments.[29,30]

B. Design of bandwidth profile and filter

To obtain the LTV filter, the temporal locations of high-frequency content are essential. In this paper, the modulus maximum of wavelet coefficients,[33] which contains the information of peak variation and singularity, is calculated to detect the characteristic values of errors based on DWT. For a signal $e(k)$, if the time $t_h = k$ is the modulus maximum point for a set of wavelet coefficients cD_q, it should meet the condition with

$$\begin{aligned} &\left|cD_q(t_h)\right| \geq \left|cD_q(t_h - 1)\right| \ and \ \left|cD_q(t_h)\right| \geq \left|cD_q(t_h + 1)\right|, \\ &\left|cD_q(t_h)\right| > \left|cD_q(t_h - 1)\right| \ or \ \left|cD_q(t_h)\right| > \left|cD_q(t_h + 1)\right|. \end{aligned} \tag{19}$$

A 4-level wavelet decomposition and corresponding detail coefficients of a 20 Hz triangle wave tracking errors with a 2.5 kHz sample rate is showed in Fig. 4. It should be noted that the high-frequency information exists in all the detail coefficients and the selection of cD_q should be deliberated. In general, cD_1 should not be taken into consideration because the high frequency noise may deteriorate the calculated results. Moreover, to make the peak of the modulus maximum to be

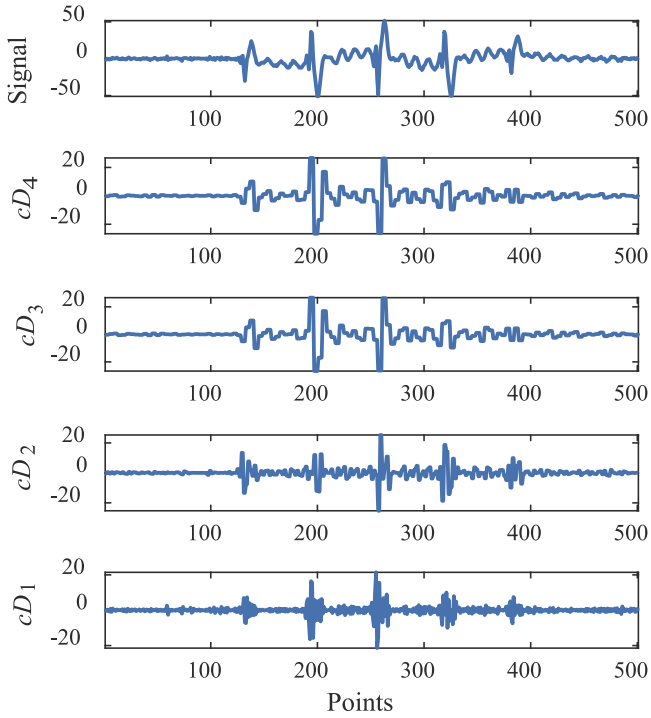

FIG. 4. A 4-level wavelet decomposition and corresponding detail coefficients.

identified more clearly and remove the burr caused by noise, the envelope of the modulus maximum is calculated by the Hilbert transform to smooth the curve by MATLAB function *envelope*. Figure 5 is the result of the smoothed modulus maximum curve of cD_2 with frequency range 312.5 Hz–625 Hz in Fig. 4 and t_1, t_2, t_3, t_4, and t_5 are the locations of the peak and singularity, i.e., the first five high-frequency locations. In practice, the number of high-frequency locations l can be determined by the references easily.

According to the location t_n determined by the modulus maximum of wavelet coefficients, the parameterized time-varying bandwidth profile is constructed in Fig. 6. $t_1, t_2, \ldots, t_n$ are the center points with width W for a high bandwidth ω_h and for other points, the bandwidth of the Q-filter is lower,

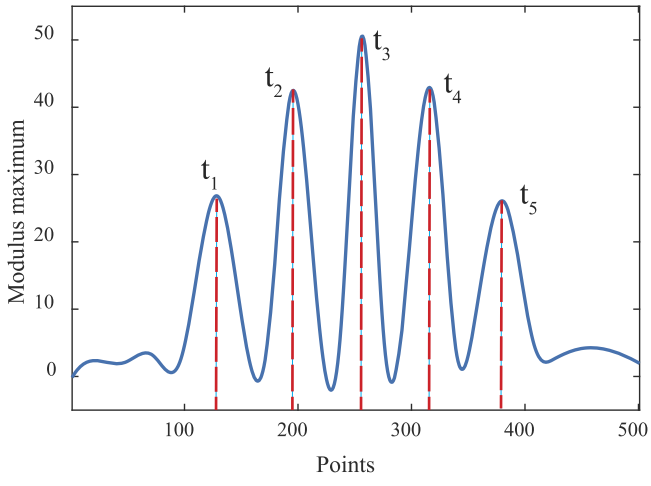

FIG. 5. Smoothed modulus maximum curve of cD_2.

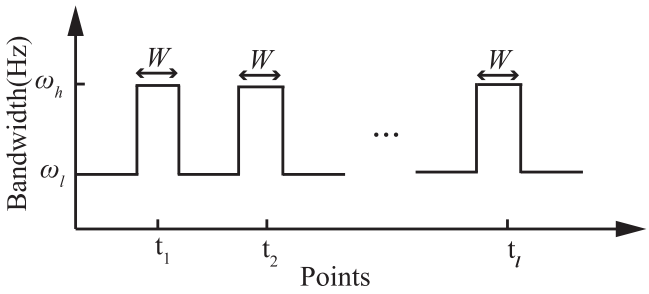

FIG. 6. Parametrized time-varying bandwidth profile for a Q-filter.

donated by ω_l. For simplicity, the width W, high bandwidth ω_h, and low bandwidth ω_l are fixed for all high frequency locations. Therefore, the bandwidth profile can be expressed as

$$\Omega(k)_i = \begin{cases} \omega_h, & t_h - W/2 \le k \le t_h + W/2, \\ \omega_l, & \text{others} \end{cases} \quad h \in \{1, 2, ..., l\}\ . \tag{20}$$

The bandwidth may change very fast for particular references. The fast switching between high and low cut-off frequency may result in the instability of the system.[17] In this regard, the bandwidth profile is smoothed by a low-pass zero-phase Gaussian filter with a cut-off frequency at 150 Hz to guarantee the smooth transition between ω_h and ω_l.

Based on the bandwidth profile, a zero-phase Butterworth filter is adopted to obtain the filtered signal without phase lag. A forward-backward filter scheme is utilized for the fast computation in practice.[34] After filtering the signal, the sequence is reversed in time and filtered by a Butterworth filter. By reversing the signal again, the original is filtered without phase distortion. This process can be performed by the MATLAB function *filtfilt*. To perform the forward-backward filter scheme on a filter with varying bandwidth, a moving-window is also introduced for each points to be filtered.[35] Through adding zeros before and after the input signal, applying the window to obtain the corresponding sequence, and filtering it by corresponding bandwidth for every point, a zero-phase sequence filtered by the LTV filter is obtained. It should be noted that the length of the moving-window cannot be too short for end-effect of the zero-phase filter.

C. Convergence analysis

Due to the LTV Q-filter, the convergence of wavelet transform-based projection ILC is analyzed in lifted domain and the LTV filter can be denoted as

$$\boldsymbol{Q_{LTV}} = \begin{bmatrix} h_{\Omega(1)}(0) & 0 & \dots & 0 \\ h_{\Omega(2)}(1) & h_{\Omega(2)}(0) & \dots & 0 \\ \vdots & \vdots & \vdots & \vdots \\ h_{\Omega(N)}(N-1) & h_{\Omega(N)}(N-2) & \dots & h_{\Omega(N)}(0) \end{bmatrix}, \tag{21}$$

where $h_{\Omega(k)}(k-1)$, $k \in \{1, 2, \dots, N\}$ are the impulse response of the Butterworth filter with bandwidth $\Omega(k)$ at time instant k.

Therefore, according to Fig. 4, the control force at iteration $i+1$ is given by

$$\boldsymbol{uff}_{i+1}^{proj} = \boldsymbol{C_{ff}}\boldsymbol{r}_{i+1}. \tag{22}$$

Substituting Eq. (15), it follows that

$$\boldsymbol{uff}_{i+1}^{proj} = (\boldsymbol{\psi}_{\boldsymbol{SPr}_i}^T \boldsymbol{\psi}_{\boldsymbol{SPr}_i})^{-1} \boldsymbol{\psi}_{\boldsymbol{SPr}_i}^T \boldsymbol{SP} \boldsymbol{\psi}_{\boldsymbol{r}_{i+1}} \boldsymbol{uff}_{i+1}, \tag{23}$$

with $\boldsymbol{\psi}_{\boldsymbol{r}_{i+1}} = [\boldsymbol{\psi}_1 \boldsymbol{r}_{i+1}, \boldsymbol{\psi}_2 \boldsymbol{r}_{i+1}, \dots, \boldsymbol{\psi}_n \boldsymbol{r}_{i+1}]$. By using Eq. (23) and the control law of traditional ILC, Eq. (22) can be rewritten as

$$\boldsymbol{uff}_{i+1}^{proj} = (\boldsymbol{\psi}_{\boldsymbol{SPr}_i}^T \boldsymbol{\psi}_{\boldsymbol{SPr}_i})^{-1} \boldsymbol{\psi}_{\boldsymbol{SPr}_i}^T \boldsymbol{SP} \boldsymbol{\psi}_{\boldsymbol{r}_{i+1}} \boldsymbol{Q}_{LTV} (\boldsymbol{uff}_i^{proj} + \boldsymbol{Le}_i). \tag{24}$$

Combining Eq. (6) yields

$$\begin{aligned} \boldsymbol{uff}_{i+1}^{proj} = {} & (\boldsymbol{\psi}_{\boldsymbol{SPr}_i}^T \boldsymbol{\psi}_{\boldsymbol{SPr}_i})^{-1} \boldsymbol{\psi}_{\boldsymbol{SPr}_i}^T \boldsymbol{SP} \boldsymbol{\psi}_{\boldsymbol{r}_{i+1}} \\ & \times \boldsymbol{Q}_{LTV} ((\boldsymbol{I} - \boldsymbol{LSP}) \boldsymbol{uff}_i^{proj} - \boldsymbol{LSr}_i). \end{aligned} \tag{25}$$

Assuming that $r_{i+1} = r_i$, the first part of Eq. (25) is equivalent as

$$(\boldsymbol{\psi}_{\boldsymbol{SPr}_i}^T \boldsymbol{\psi}_{\boldsymbol{SPr}_i})^{-1} \boldsymbol{\psi}_{\boldsymbol{SPr}_i}^T \boldsymbol{SP} \boldsymbol{\psi}_{\boldsymbol{r}_{i+1}} = \boldsymbol{\psi}_{\boldsymbol{SPr}_i} (\boldsymbol{\psi}_{\boldsymbol{SPr}_i}^T \boldsymbol{\psi}_{\boldsymbol{SPr}_i})^{-1} \boldsymbol{\psi}_{\boldsymbol{SPr}_i}^T, \tag{26}$$

which is obtained because that causality of $S(z)P(z)$ and $\boldsymbol{\psi}_j$ implies that $\boldsymbol{SP}$ and $(\boldsymbol{\psi}_{\boldsymbol{SPr}_i}^T \boldsymbol{\psi}_{\boldsymbol{SPr}_i})^{-1} \boldsymbol{\psi}_{\boldsymbol{SPr}_i}^T$ can commute each other.[26] According to the definition of the projection matrix, $\boldsymbol{\psi}_{\boldsymbol{SPr}_i} (\boldsymbol{\psi}_{\boldsymbol{SPr}_i}^T \boldsymbol{\psi}_{\boldsymbol{SPr}_i})^{-1} \boldsymbol{\psi}_{\boldsymbol{SPr}_i}^T$ is a projection matrix with $\bar{\sigma}(\boldsymbol{\psi}_{\boldsymbol{SPr}_i} (\boldsymbol{\psi}_{\boldsymbol{SPr}_i}^T \boldsymbol{\psi}_{\boldsymbol{SPr}_i})^{-1} \boldsymbol{\psi}_{\boldsymbol{SPr}_i}^T) = 1$, where $\bar{\sigma}$ denotes the maximum singular value of the matrix.

Therefore, combining Eqs. (25) and (26), the control signal is convergent if

$$\begin{aligned} & \bar{\sigma} ((\boldsymbol{\psi}_{\boldsymbol{SPr}_i}^T \boldsymbol{\psi}_{\boldsymbol{SPr}_i})^{-1} \boldsymbol{\psi}_{\boldsymbol{SPr}_i}^T \boldsymbol{SP} \boldsymbol{\psi}_{\boldsymbol{r}_{i+1}} \boldsymbol{Q}_{LTV} (\boldsymbol{I} - \boldsymbol{LSP}) \\ & \quad = \bar{\sigma} (\boldsymbol{\psi}_{\boldsymbol{SPr}_i} (\boldsymbol{\psi}_{\boldsymbol{SPr}_i}^T \boldsymbol{\psi}_{\boldsymbol{SPr}_i})^{-1} \boldsymbol{\psi}_{\boldsymbol{SPr}_i}^T \boldsymbol{Q}_{LTV} (\boldsymbol{I} - \boldsymbol{LSP}) \\ & \quad = \bar{\sigma} (\boldsymbol{\psi}_{\boldsymbol{SPr}_i} (\boldsymbol{\psi}_{\boldsymbol{SPr}_i}^T \boldsymbol{\psi}_{\boldsymbol{SPr}_i})^{-1} \boldsymbol{\psi}_{\boldsymbol{SPr}_i}^T) \bar{\sigma} (\boldsymbol{Q}_{LTV} (\boldsymbol{I} - \boldsymbol{LSP})) \\ & \quad = \bar{\sigma} (\boldsymbol{Q}_{LTV} (\boldsymbol{I} - \boldsymbol{LSP})) < 1. \end{aligned} \tag{27}$$

It can be concluded that the convergence of the LTV Q-filter projection ILC relies on the design of the learning filter and LTV filter, which is similar to the traditional frequency-domain ILC. To meet the convergence condition, the bandwidth profile should be designed subtly.

D. Design procedure

Herein, the design procedure demonstrated in Fig. 7 is proposed for high-bandwidth and flexible tracking, which represents the main contributions of this paper.

Before it is implemented, the feedforward controller is initialized by setting $\boldsymbol{\theta}_0 = 0$, $\boldsymbol{uff}_0^{proj}(k) = \boldsymbol{0}$. The parameters ω_l, ω_h, and W are determined beforehand to meet the convergence condition. The learning filter $L(z)$ can be designed by the method in traditional frequency-domain ILC, such as the approximate inversion approach.

It should be noted that for *Step* (2) in Fig. 7, DWT depends strongly on the choice of the wavelet function. In this paper, the optimal wavelet function is determined based on the maximum errors between a reference error obtained by the experiment

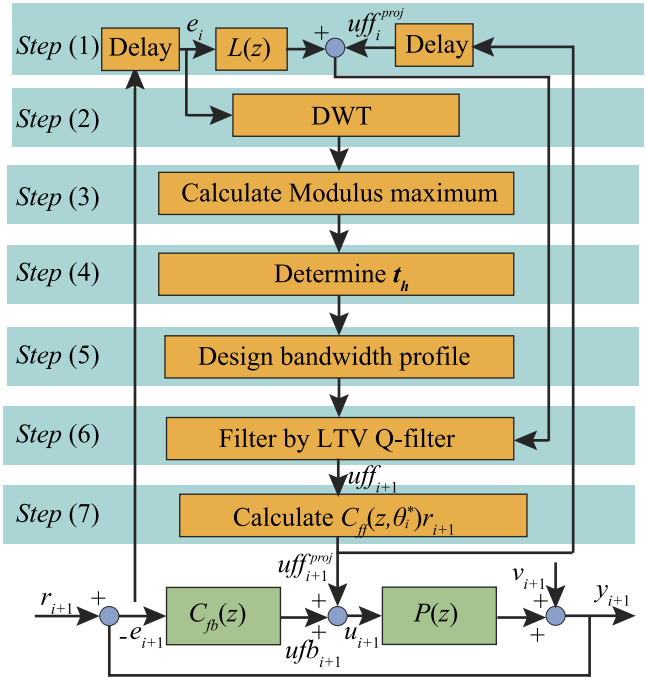

FIG. 7. Design procedure of the wavelet transform-based LTV filter design for projection ILC.

without a feedforward controller and a reconstructed error signal with DWT.[29] The control signal for next iteration can be calculated according to Eqs. (22) and (23) in *Step* (6).

Besides, it is clear that a key assumption of the proposed approach in Fig. 7 is that the references should be planned in advance in order to calculate the control force of next iteration. However, the assumption can be met easily in many real applications, such as the precision motion in nanopositioning,[36] wafer stages,[17,27] semiconductor bonding equipment,[26] and a flatbed inkjet printer[37] where the varying references are known ahead before implementation.

IV. APPLICATION TO A PIEZO NANOPOSITIONER

A. Experimental setup

A three-axis nanopositioner (P-561.3CD, Physik Instrumente) was developed to verify the proposed method. In this paper, only the x axis with a stoke of 100 μm was experimented for comparisons. The control input voltage (0–10 V) is produced by 16-bit digital to analog converters (DACs) of the data acquisition card (PCI 6289, National Instrument) and subsequently amplified via a piezo amplifier module (E-503.00, Physik Instrumente) with a fixed gain of 10 to provide excitation voltage (0–100 V) for the nanopositioner. The output (0–10 V), which is normalized with respect to 0–100 μm, is read via a sensor monitor (E-509.C3A, Physik Instrumente) and is passed to the data acquisition card (PCI 6289, National Instrument). The control system of the nanopositioning stage is developed based on Simulink Real-Time in MATLAB/Simulink environment. The control algorithm was designed in a Matlab/Simulink block diagram on a development PC and executed in real-time on the target PC (CPU: Intel Core i5 @3.3 GHz) after compiling. In this paper, the sample

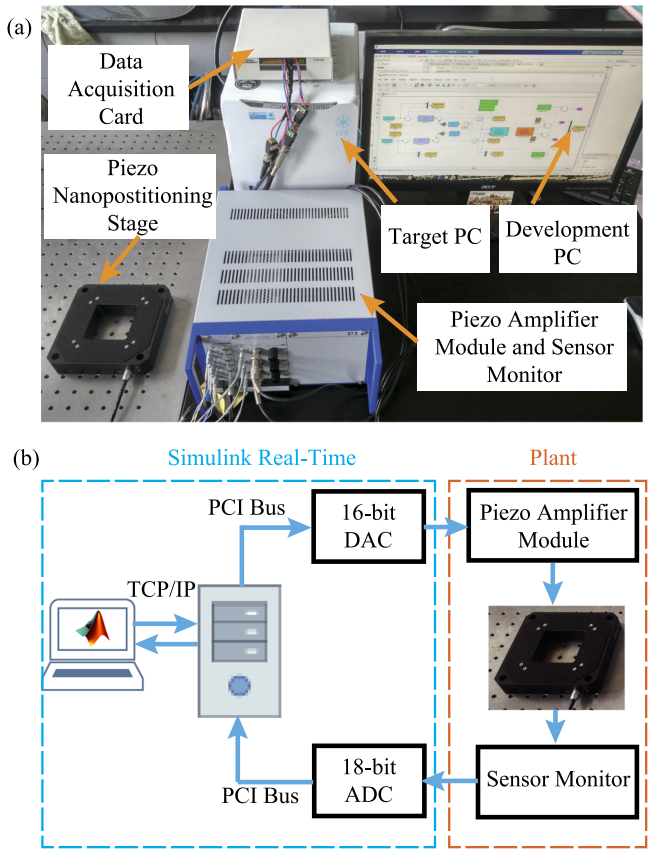

FIG. 8. The experimental setup of nanopositioner (a) experimental platform and (b) block diagram of the control system.

rate is set to 2.5 kHz. The overall experimental setup of the system is showed in Fig. 8.

To obtain the dynamic model, a sine-sweep input voltage with a constant amplitude of 200 mV between 0.1 Hz and 500 Hz was applied to the x axis. It should be noted that the low amplitude voltage was used to excite the system to avoid distortion from hysteresis.[38] The model was identified by the system identification toolbox in MATLAB via the function *tfest*. Through being discretized via a zero-order holder (ZOH) method, the linear discrete transfer function $P(z)$ was obtained as

$$P(z) = \frac{0.0128z^4 - 0.055z^3 + 0.113z^2 - 0.108z + 0.0417}{z^5 - 4.11z^4 + 7.09z^3 - 6.382z^2 + 2.983z - 0.5796}. \tag{28}$$

The identified and measured frequency response is plotted in Fig. 9, which indicates that Eq. (28) captures the dynamics of the stage well.

B. Controller implementation

To eliminate the effect of hysteresis, a high-gain feedback controller was also designed primarily. The notch filter can improve the stability margin, and then a high-gain integral controller was developed to suppress the hysteresis.[38] The controller $C_{fb}(z)$ was obtained by discretizing via a ZOH method as

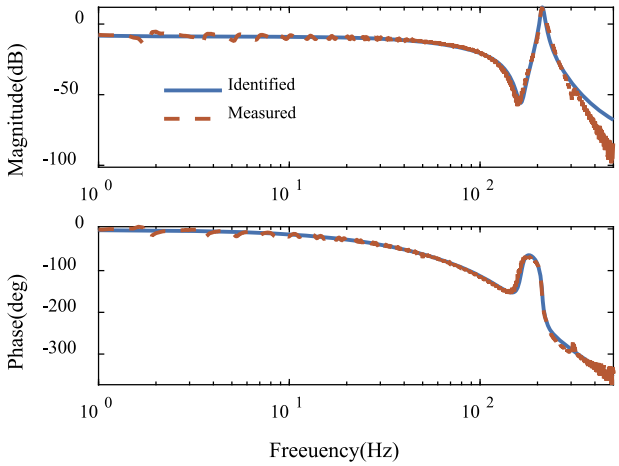

FIG. 9. Frequency response of the piezo nanopositioner.

$$C_{fb}(z) = \frac{0.05239z^3 - 0.03764z^2 - 0.03892z + 0.05112}{z^3 - 2.355z^2 + 2.226z - 0.871}. \tag{29}$$

Experimental results of hysteresis curves with and without a feedback controller is displayed in Fig. 10. For a triangular wave with 2 μm amplitude, the maximal errors are 0.1172 μm (5.86% of the maximum magnitude) and 0.019 μm (0.95% of the maximum magnitude), respectively, which demonstrates that the high-gain feedback controller can suppress hysteresis significantly. Therefore, the effect of hysteresis nonlinearity is neglected in this paper.

For the implementation of the proposed wavelet transform-based projection ILC, the overall design procedure in Fig. 7 was adopted. The learning filter $L(z)$ was designed by a zero-phase-error tracking controller (ZPETC)[39] to approximate $P(z)/(S(z)P(z))$ in this paper and the Butterworth filter was utilized as the Q-filter, which can be designed with different cut-off frequencies easily by MATLAB function *butter*. A fourth-order low-pass Butterworth filter was used for experiments. The order of the parameterized FIR filter $C_{ff}(z)$ was set to $n = 10$ in this paper. Besides, the wavelet function "db1" was adopted to calculate the 4-level wavelet decomposition. For the design of the bandwidth profile, the low bandwidth, high bandwidth, and width were selected as $\omega_l = 100$ Hz, $\omega_h = 250$ Hz,

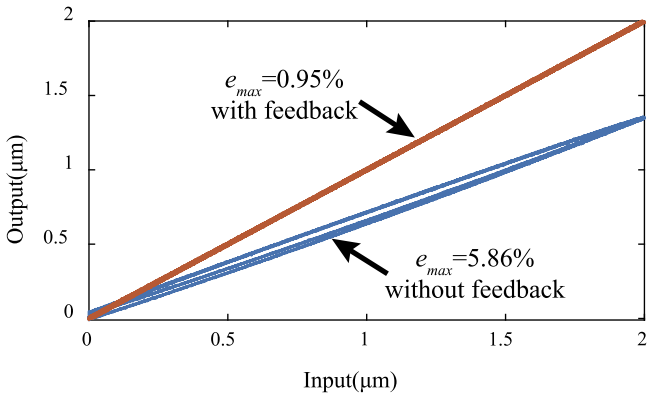

FIG. 10. Experimental results of hysteresis suppression by a high-gain feedback controller.

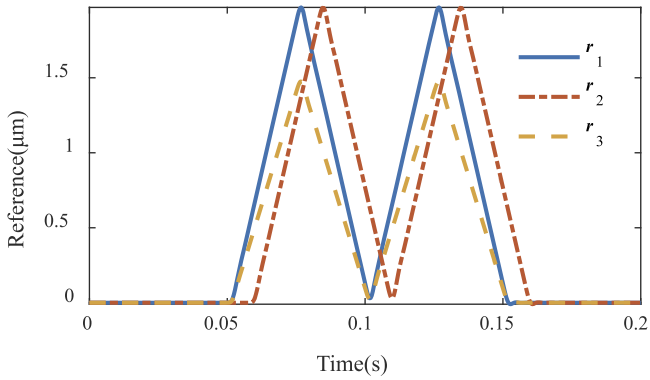

FIG. 11. References for experiments.

and $W = 20$, respectively, which are pre-designed through simulation. The bandwidth profile can be obtained by Eq. (20) and the control signal was calculated by projecting the filtered zero-phase signal according to Fig. 7.

C. Results of triangular waves tracking

Triangular waves, which are usually used for raster scanning in a nanopositioner, were adopted as the references.

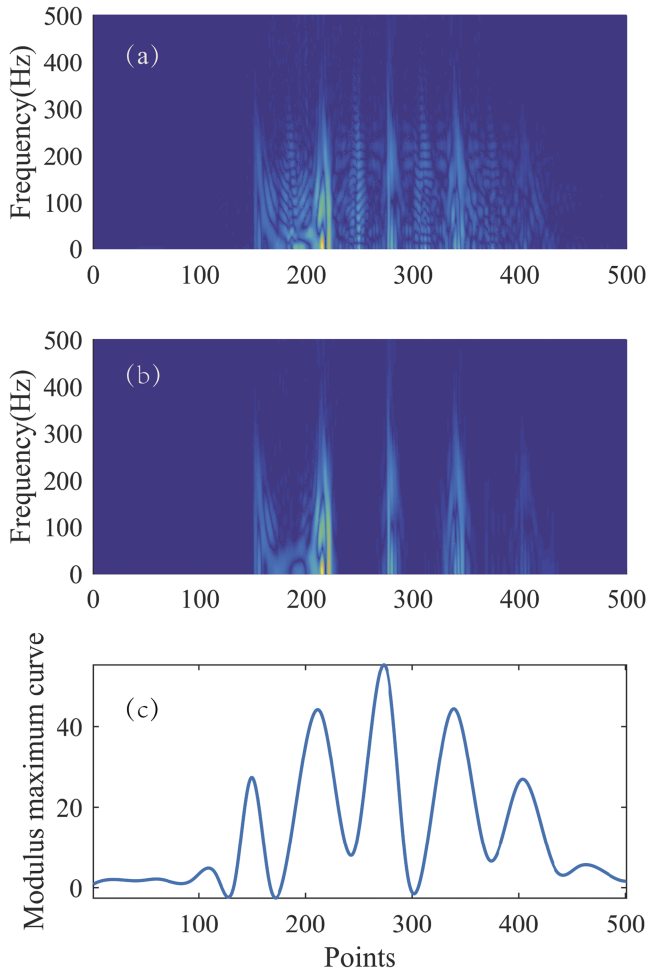

FIG. 12. Comparisons of time-frequency decomposition for errors at 15th iteration of projection ILC. (a) Wigner-Ville time-frequency distribution, (b) piece-wise Wigner-Ville time-frequency distribution, and (c) modulus maximum based on DWT.

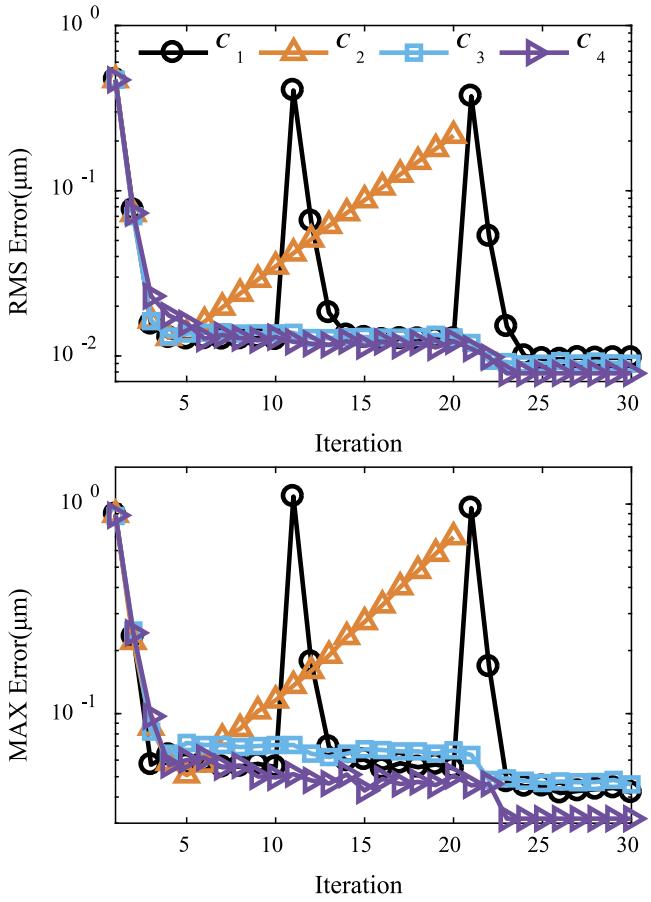

FIG. 13. Experiments results of RMS and MAX errors with 30 iterations.

Three references defined for experiments are depicted in Fig. 11, where $\boldsymbol{r}_1$ for the 1th–10th iterations are 20 Hz triangular waves with the amplitude of 2 μm, $\boldsymbol{r}_2$ for the 11th–20th iterations have a 0.01 s delay with respect to $\boldsymbol{r}_1$, and $\boldsymbol{r}_3$ for the 21th–30th iterations are generated through multiplying $\boldsymbol{r}_1$ by 0.75. Furthermore, four feedforward controllers listed below have also been developed for comparisons.

(1) $\boldsymbol{C}_1$: the traditional frequency-domain ILC[14] with a Q-filter with cut-off frequency at 120 Hz.
(2) $\boldsymbol{C}_2$: the traditional frequency-domain ILC with a Q-filter with cut-off frequency at 240 Hz.
(3) $\boldsymbol{C}_3$: the projection ILC[26] with a Q-filter with cut-off frequency at 120 Hz.
(4) $\boldsymbol{C}_4$: the projection ILC with a LTV Q-filter based on wavelet transform proposed in this paper.

TABLE I. Statistical results of errors at iterations with changing references.

Errors	Controllers	RMS errors (nm)	MAX errors (nm)
$\boldsymbol{e}_{11}$	$\boldsymbol{C}_1$	404.30	1085.00
	$\boldsymbol{C}_3$	13.80	70.84
	$\boldsymbol{C}_4$	12.18	51.41
$\boldsymbol{e}_{21}$	$\boldsymbol{C}_1$	327.90	955.30
	$\boldsymbol{C}_3$	11.98	63.50
	$\boldsymbol{C}_4$	11.08	45.46

1. Time-frequency analysis

In order to validate the accuracy of high-frequency locations determined by DWT, the time-frequency decomposition of errors at the 15th iteration of projection ILC was analyzed in Fig. 12. It is clear that the cross-terms exist at points 184, 248, 311, and 368, respectively, in Fig. 12(a), which is the main deficiency of Wigner-Ville time-frequency distribution. Besides, as the signal components increase, the additional cross-terms become more and more in the spectrum, which may result in confusing with the real high-frequency locations. In Ref. 17, the piecewise clipping algorithm by cutting the signal into pieces was used to eliminate cross-terms. Although piecewise Wigner-Ville time-frequency distribution can remove the effect of cross-terms, each piece must contain only one peak and the process to segment the signal should be done manually, which is impractical during iterations for varying references. The smoothed modulus maximum curve of cD_2 with 4-level discrete wavelet decomposition is showed in Fig. 12(c). Compared with Wigner-Ville time-frequency distribution, DWT avoids the cross-terms. Moreover, it is practical to implement DWT after each iteration automatically for flexible tracking. The high-frequency regions in Fig. 12(b) are located at $t_h = \{152, 215, 278, 342, 406\}$ and the locations of the modulus maximum calculated by DWT are $t_h = \{149, 211, 273, 339, 404\}$, which demonstrates that the proposed method can locate the high-frequency regions accurately.

2. Tracking performance

Thirty iterations with varying references were performed to demonstrate the advantage of the proposed method on high-bandwidth and flexible tracking.

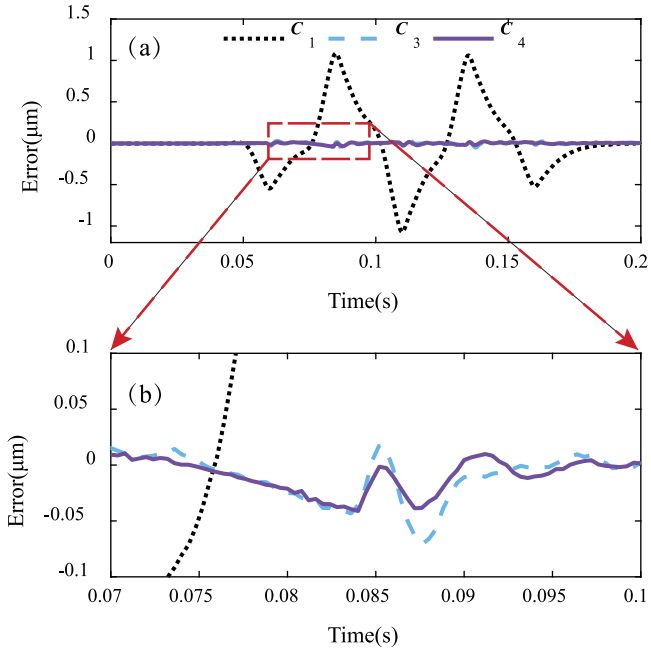

FIG. 14. Experiment results of $\boldsymbol{r}_2$ at the 20th iteration using different controllers. (a) Tracking errors (b) zoomed-in view of the tracking errors.

TABLE II. Statistical results of convergent errors for different references.

Reference	Controllers	RMS errors (nm)	MAX errors (nm)
	$\boldsymbol{C}_1$	12.55	55.58
$\boldsymbol{r}_1$	$\boldsymbol{C}_3$	13.70	70.84
	$\boldsymbol{C}_4$	13.00	49.63
	$\boldsymbol{C}_1$	12.91	60.31
$\boldsymbol{r}_2$	$\boldsymbol{C}_3$	13.04	67.63
	$\boldsymbol{C}_4$	11.48	42.95
	$\boldsymbol{C}_1$	9.73	44.17
$\boldsymbol{r}_3$	$\boldsymbol{C}_3$	8.98	48.26
	$\boldsymbol{C}_4$	7.85	31.54

The Root-Mean-Square (RMS) errors and maximal (MAX) errors during iterations are showed in Fig. 13. Compared with $\boldsymbol{C}_1$, $\boldsymbol{C}_2$ can achieve smaller errors at first five iterations, but the errors become diverged subsequently. Although a Q-filter with higher cut-off frequency can improve the high-bandwidth tracking performance, the convergence cannot be guaranteed for magnifying the noise and non-repetitive disturbances. Therefore, the bandwidth of the Q-filter should not be too high in practice, which limits the high-bandwidth tracking in turn. Both $\boldsymbol{C}_3$ and $\boldsymbol{C}_4$ have the ability for varying references tracking, which can be concluded from Fig. 13 and Table I, especially at 11th and 21th iterations. The RMS error of $\boldsymbol{C}_1$ is 404.30 nm, while the RMS errors with $\boldsymbol{C}_3$ and $\boldsymbol{C}_4$ are 13.80 nm and 12.18 nm, respectively, at the 11th iteration, which indicates that $\boldsymbol{C}_3$ and $\boldsymbol{C}_4$ are not sensitive to changes between iterations. The similar conclusion can also be obtained at the 21th iteration.

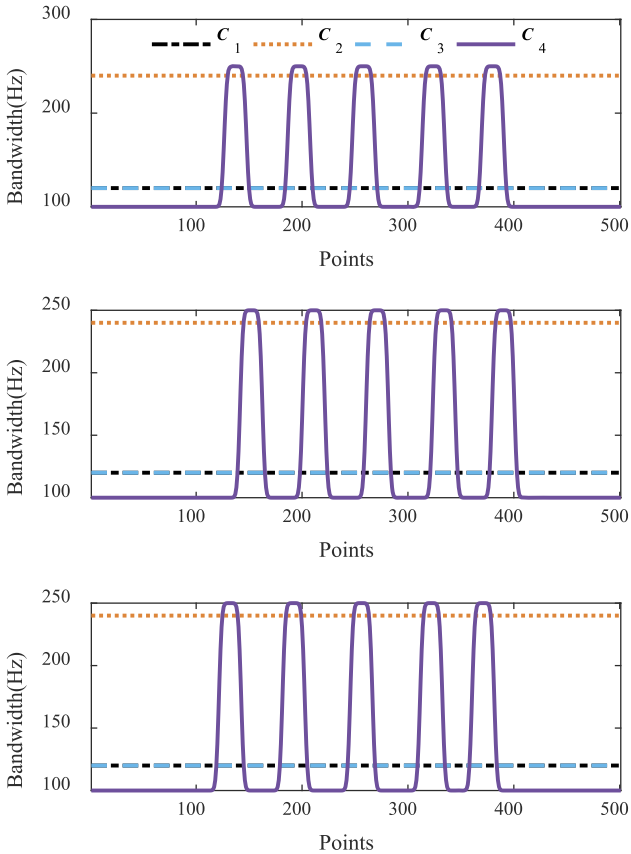

FIG. 15. Calculated bandwidth profiles of different controllers. (a) Bandwidth profiles at the 7th iteration, (b) bandwidth profiles at the 14th iteration, and (c) bandwidth profiles at the 28th iteration.

The proposed controller $\boldsymbol{C}_4$ can also handle high-bandwidth tracking, which is presented in Fig. 14 and Table II. Although reducing RMS errors lightly, the proposed method can improve the tracking performance with high-frequency components in comparison with $\boldsymbol{C}_3$. The statistical results of MAX convergent errors confirm the conclusion. Take the tracking results of $\boldsymbol{r}_2$ at the 20th iteration as an example. The MAX error with $\boldsymbol{C}_4$ reduces 36.49% (from 37.36 nm to 42.95 nm) with respect to the MAX error implementing $\boldsymbol{C}_3$, which demonstrates that the high-frequency errors were compensated by the proposed LTV filter. More detailed data can be found in Table II.

The calculated bandwidth profiles based on DWT during iterations for different references are showed in Fig. 15. The high-frequency locations at the 7th, 14th, and 28th iterations are $t_h = \{137, 197, 258, 324, 380\}$, $t_h = \{152, 211, 271, 334, 390\}$, and $t_h = \{132, 192, 258, 322, 371\}$, respectively. Therefore, the proposed method can detect the change of high-frequency locations of errors and adjust the bandwidth profile accordingly between iterations to achieve high-bandwidth and flexible tracking simultaneously.

V. CONCLUSION

In this paper, a wavelet transform-based LTV Q-filter design for projection ILC was developed considering high-bandwidth and flexible tracking for precision motion. First, the design method for LTV bandwidth profiles was proposed to isolate the high-frequency locations based on the modulus maximum of wavelet detail coefficients calculated by DWT. Then, the projection ILC with a LTV Q-filter was constructed, which significantly improves the performance of high-bandwidth and flexible tracking. Moreover, the wavelet transform-based method avoids the cross-terms and segmenting manually for general time-frequency decomposition. To validate the performance, the proposed method was implemented on a piezo nanopositioner. Experimental results show that the wavelet transform-based method can locate the high-frequency regions accurately compared with Wigner-Ville and piece-wise Wigner-Ville time-frequency distribution. For 20 Hz triangular waves varying during iterations, the proposed controller can handle the varying references and compensate high-frequency errors by comparing with traditional ILC and projection ILC with a fixed-bandwidth Q-filter.

The future work will take the effect of hysteresis nonlinearity into consideration, especially for the large stroke of the nanopositioner and extend this approach to multiple-input-multiple-output (MIMO) systems. Besides, the method depends on the accurate model, and a non-model based approach[40] can also be explored in the next stage.

ACKNOWLEDGMENTS

This work was supported by the Natural Science Foundation of China under Grant No. 51375349 and Shenzhen Science and Technology Program under Grant No. JCYJ20170306171514468.

[1]G. Binnig, C. F. Quate, and C. Gerber, "Atomic force microscope," Phys. Rev. Lett. **56**, 930 (1986).
[2]I. Horcas, R. Fernández, J. M. Gómezrodríguez, J. Colchero, J. Gómezherrero, and A. M. Baro, "WSXM: A software for scanning probe microscopy and a tool for nanotechnology," Rev. Sci. Instrum. **78**, 013705 (2007).
[3]H. Lan, Y. Ding, H. Liu, and B. Lu, "Review of the wafer stage for nanoimprint lithography," Microelectron. Eng. **84**, 684–688 (2007).
[4]E. Eleftheriou, T. Antonakopoulos, G. Binnig, G. Cherubini, M. Despont, A. Dholakia, U. Durig, M. Lantz, H. Pozidis, and H. Rothuizen, "Millipede-a MEMS-based scanning-probe data-storage system," IEEE Trans. Magn. **39**, 938–945 (2003).
[5]S. M. Salapaka, A. Sebastian, J. P. Cleveland, and M. V. Salapaka, "High bandwidth nano-positioner: A robust control approach," Rev. Sci. Instrum. **73**, 3232–3241 (2002).
[6]Y. K. Yong, S. O. R. Moheimani, B. J. Kenton, and K. K. Leang, "High-speed flexure-guided nanopositioning: Mechanical design and control issues," Rev. Sci. Instrum. **83**, 121101 (2012).
[7]M. Fairbairn and S. O. R. Moheimani, "Resonant control of an atomic force microscope micro-cantilever for active Q control," Rev. Sci. Instrum. **83**, 083708 (2012).
[8]I. A. Mahmood and S. O. R. Moheimani, "Making a commercial atomic force microscope more accurate and faster using positive position feedback control," Rev. Sci. Instrum. **80**, 063705 (2009).
[9]B. Bhikkaji and S. O. Moheimani, "Integral resonant control of a piezoelectric tube actuator for fast nanoscale positioning," IEEE/ASME Trans. Mechatronics **13**, 530–537 (2008).
[10]Y. Wu and Q. Zou, "Robust inversion-based 2-DOF control design for output tracking: Piezoelectric-actuator example," IEEE Trans. Control Syst. Technol. **17**, 1069–1082 (2009).
[11]C. Lee and S. M. Salapaka, "Robust broadband nanopositioning: Fundamental trade-offs, analysis, and design in a two-degree-of-freedom control framework," Nanotechnology **20**, 035501 (2009).
[12]G. M. Clayton, S. Tien, K. K. Leang, Q. Zou, and S. Devasia, "A review of feedforward control approaches in nanopositioning for high-speed SPM," J. Dyn. Syst., Meas., Control **131**, 061101 (2009).
[13]S. Devasia, E. Eleftheriou, and S. O. R. Moheimani, "A survey of control issues in nanopositioning," IEEE Trans. Control Syst. Technol. **15**, 802–823 (2007).
[14]D. A. Bristow, M. Tharayil, and A. Alleyne, "A survey of iterative learning control," IEEE Control Syst. Mag. **26**, 96–114 (2006).
[15]H. Ahn, Y. Chen, and K. L. Moore, "Iterative learning control brief survey and categorization," IEEE Trans. Syst. Man Cybern. **37**, 1099–1121 (2007).
[16]H. Sun and A. G. Alleyne, "A computationally efficient norm optimal iterative learning control approach for LTV systems," Automatica **50**, 141–148 (2014).
[17]I. Rotariu, M. Steinbuch, and R. Ellenbroek, "Adaptive iterative learning control for high precision motion systems," IEEE Trans. Control Syst. Technol. **16**, 1075–1082 (2008).
[18]D. A. Bristow, J. Dong, A. G. Alleyne, P. Ferreira, and S. Salapaka, "High bandwidth control of precision motion instrumentation," Rev. Sci. Instrum. **79**, 103704 (2008).
[19]D. A. Bristow, A. G. Alleyne, and M. Tharayil, "Optimizing learning convergence speed and converged error for precision motion control," J. Dyn. Syst., Meas., Control **130**, 054501 (2008).
[20]D. J. Hoelzle, A. Alleyne, and A. J. W. Johnson, "Basis task approach to iterative learning control with applications to micro-robotic deposition," IEEE Trans. Control Syst. Technol. **19**, 1138–1148 (2011).
[21]M.-B. Radac and R.-E. Precup, "Optimal behaviour prediction using a primitive-based data-driven model-free iterative learning control approach," Comput. Ind. **74**, 95–109 (2015).
[22]S. H. V. D. Meulen, R. L. Tousain, and O. H. Bosgra, "Fixed structure feedforward controller design exploiting iterative trials: Application to a wafer stage and a desktop printer," J. Dyn. Syst., Meas., Control **130**, 051006 (2008).
[23]M. F. Heertjes and A. Van Engelen, "Minimizing cross-talk in high-precision motion systems using data-based dynamic decoupling," Control Eng. Pract. **19**, 1423–1432 (2011).
[24]J. Bolder and T. Oomen, "Rational basis functions in iterative learning control—With experimental verification on a motion system," IEEE Trans. Control Syst. Technol. **23**, 722–729 (2015).
[25]J. Van Zundert, J. Bolder, and T. Oomen, "Optimality and flexibility in iterative learning control for varying tasks," Automatica **67**, 295–302 (2016).
[26]F. Boeren, A. Bareja, T. Kok, and T. Oomen, "Frequency-domain ILC approach for repeating and varying tasks: With application to semiconductor bonding equipment," IEEE/ASME Trans. Mechatronics **21**, 2716–2727 (2016).
[27]S. Mishra and M. Tomizuka, "Projection-based iterative learning control for wafer scanner systems," IEEE/ASME Trans. Mechatronics **14**, 388–393 (2009).
[28]Y. Ye and D. Wang, "DCT basis function learning control," IEEE/ASME Trans. Mechatronics **10**, 449–454 (2005).
[29]R. Merry, R. V. De Molengraft, and M. Steinbuch, "Iterative learning control with wavelet filtering," Int. J. Robust Nonlinear Control **18**, 1052–1071 (2008).
[30]J. Cui, F. Zhao, Z. Chu, and S. S. Ge, "Experiment on trajectory tracking control of high precise positioning system based on iterative learning controller with wavelet filtering," Mechatronics **32**, 88–95 (2015).
[31]M. Norrlöf and S. Gunnarsson, "Time and frequency domain convergence properties in iterative learning control," Int. J. Control **75**, 1114–1126 (2002).
[32]I. Daubechies, "The wavelet transform, time-frequency localization and signal analysis," IEEE Trans. Inf. Theory **36**, 961–1005 (1990).
[33]S. Mallat and W. L. Hwang, "Singularity detection and processing with wavelets," IEEE Trans Inf. Theory **38**, 617–643 (1992).
[34]F. Gustafsson, "Determining the initial states in forward-backward filtering," IEEE Trans. Signal Process. **44**, 988–992 (1996).
[35]D. Yu, Y. Zhu, K. Yang, C. Hu, and M. Li, "A time-varying Q-filter design for iterative learning control with application to an ultra-precision dual-stage actuated wafer stage," Proc. Inst. Mech. Eng., Part I: J. Syst. Control Eng. **228**, 658–667 (2014).
[36]F. Boeren, D. Bruijnen, and T. Oomen, "Enhancing feedforward controller tuning via instrumental variables: With application to nanopositioning," Int. J. Control **90**, 746–764 (2017).
[37]J. Bolder, J. Van Zundert, S. Koekebakker, and T. Oomen, "Enhancing flatbed printer accuracy and throughput: Optimal rational feedforward controller tuning via iterative learning control," IEEE Trans. Ind. Electron. **64**, 4207–4216 (2017).
[38]K. K. Leang and S. Devasia, "Feedback-linearized inverse feedforward for creep, hysteresis, and vibration compensation in AFM piezo actuators," IEEE Trans. Control Syst. Technol. **15**, 927–935 (2007).
[39]M. Tomizuka, "Zero phase error tracking algorithm for digital control," J. Dyn. Syst., Meas., Control **109**, 65–68 (1987).
[40]S. Z. Khong, D. Nesic, and M. Krstic, "Iterative learning control based on extremum seeking," Automatica **66**, 238–245 (2016).